Bounded Jet Flow Issuing from a Square Nozzle

Tsutomu NOZAKI

(Received May 30, 1981)

From the experiments of the bounded jet flow issuing from a square nozzle, it was found that the flow relatively near the nozzle exit is fairly complex according to development of the secondary flow induced by deformation and stretching of the closed vortex tube. In the region far from the nozzle exit, however, the secondary flow almost disappears. From a point of view of the extent of the secondary flow, the flow consists of three regions as was suggested by Holdeman and Foss. These are a near, middle and far field regions in which the secondary motion is initiated, developed and decayed, respectively. These regions are also observed from the isotach patterns of the bounded jet issuing from a square nozzle. In the far regions, the approximate calculations of the velocity, momentum and kinetic energy distributions based on some simple assumptions agree well with the experiments.

1. Introduction

The jet issuing from a rectangular nozzle to the space bounded by two parallel flat plates, say a bounded jet flow, can be seen in many types of fluid jet devices such as oscillators, switches or logic elements, and amplifiers or proportional elements. In such flows, structure of the bounded jet flow is so different from that of a two-dimensional jet flow [1], according to the effects of the boundary layer formed and developed on the side plates and the production of a streamwise vorticity.

Foss and Jones [2] proposed a vortex stretching model to explain the effect of the secondary flow in the bounded jet from their experiments of the flow with aspect ratio of the nozzle equal to 6. They also suggested that the flow appears to be combination of a couple of two-dimensional flows, that is, one is the flow which is considered to be a two-dimensional jet and another is the boundary layer flow on the parallel side plates.

McCabe [3] suggested from his experiments of the flow with aspect ratio equal to 3 that the flow had a three dimensional nature. The secondary flow arose in the boundary layers on the side plates and a possible explanation of the method of secondary flow generation has been proposed based on the deformation and stretching of vortex filaments convected with the mean flow.

Holdeman and Foss [4] proposed that the secondary flow in the bounded jet flow with a low aspect ratio is described in terms of a near, middle and far field regions in which the secondary motion is initiated, developed and decayed, respectively. The initiation of the secondary flow is explained by the distortion of the planner vortex loops which bound the jet at the exit plane.

Many investigations concerning the bounded jet flow have been done so far, but the calculations have not been done yet, so far as the author is aware. On the basis of the experimental results of the flow with aspect ratio equal to 1 by the author, the approximate calculations of the isotach patterns of the bounded jet are carried out for the flow far from the nozzle exit where the secondary flow is decayed, that is, in far

field region. The calculated results are compared with the experimental ones.

2. Experimental equipment and procedure

As shown in Fig. 1, let the origin O be taken at the center of the nozzle exit, the axis of x in the streamwise direction, axes of y and z in the direction perpendicular to it and the axial velocity components u, v and w, respectively. Let x-y plane denote the mid-plane and x-z plane the center-plane. U_0 denotes a uniform velocity at the nozzle exit, $2b_0$ the nozzle width, U_c the center axis velocity in the zone of established flow and $2b$ the width of the jet. Figure 2 shows the experimental apparatus. The air flow from the centerifugal blower passes through three stainless steel screens to suppress the flow turbulence and then issues from the nozzle exit with a uniform velocity profile. The nozzle with aspect ratio equal to 1 and the width 50mm are used. The nozzle contour constists of circular arcs. At the nozzle exit plane, the tangents to the circular arcs of

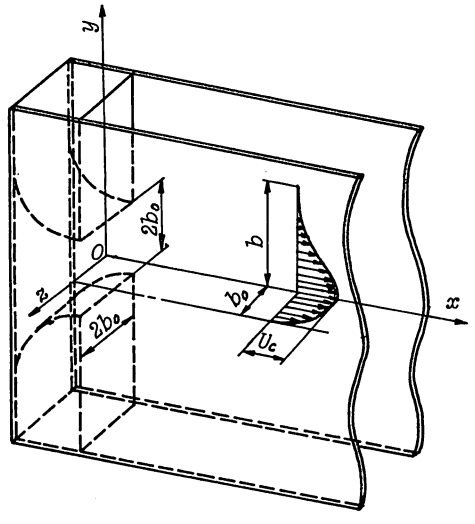

Fig. 1 Schema of a bounded jet model

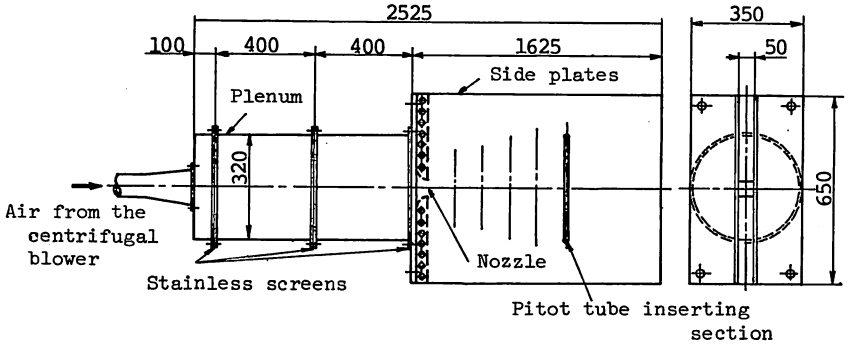

Fig. 2 Experimental apparatus

the nozzle are parallel to the jet axis. Velocities and static pressures are detected by a Pitot-cylinder and a static-tube.

3. Experimental results and discussions

3.1 Effects of Reynolds number

In order to clarify the effects of Reynolds number in the bounded jet flow, Reynolds number is defined by

$$Re=2U_0b_0/\nu \tag{1}$$

conveniently, where ν denotes a kinematic viscosity of the fluid. Figure 3 shows the isotach patterns of the bounded jet flow at $x/b_0=4$ using Reynolds number as a parameter. For $Re=2.07\times10^4$, the flow tends to concentrate to the center region of the jet, but as Reynolds number becomes large, the width of the jet becomes large in the vicinity of the side plates. This fact is verified from the experimental results of the center axis velocity decay shown in Fig. 4. As Reynolds number increases, the center axis velocity approaches to that of a two-dimensional jet flow depicted by a solid line. The behaviour

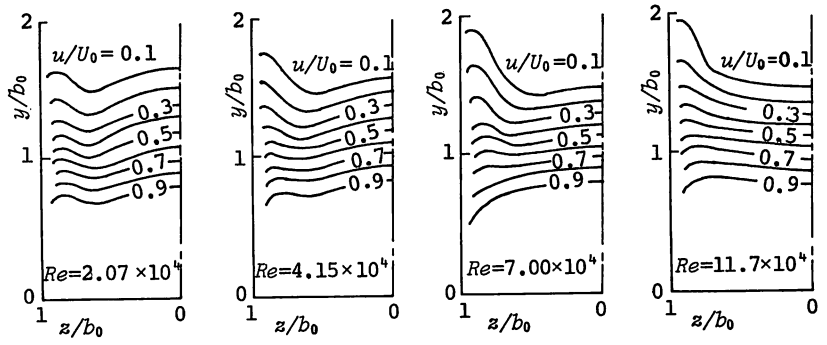

Fig. 3 Isotach patterns (Effects of Reynolds number)

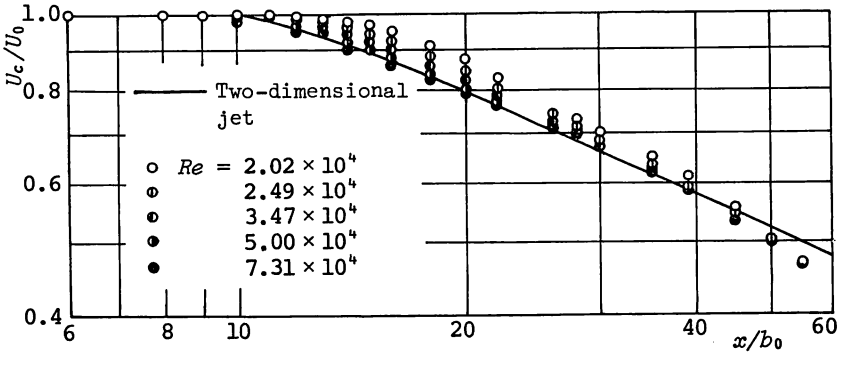

Fig. 4 Center axis velocity decays of the bounded jet

of the bounded jet flow varies with Reynolds number, then the experiments are done with the fixed Reynolds number $Re=3.47\times10^4$ for convenience.

3.2 Width of the jet in the mid-plane

Figure 5 shows the width of the jet in the mid-plane. A solid line represents the width of a two-dimensional jet for comparison. The experimental values of the bounded jet agree well with this line in the range of $x/b_o<8$. This means that the flow is considered to be two-dimensional in the mid-plane at least. The widths of the bouned jet are smaller than those of the two-dimensional jet in the region of $8\leqq x/b_o\leqq30$. In the region $x/b_o>30$, the widths of the bounded jet in the mid-plane are larger than those of the two-dimensional jet.

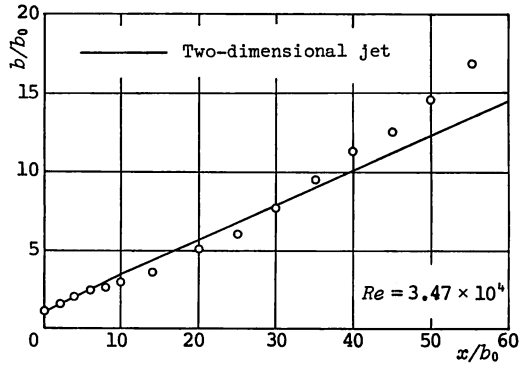

Fig. 5 Width of the jet in the mid-plane

3.3 Isotach patterns

The isotach patterns in $x-y$ plane are shown in Fig. 6. For $x/b_o=4$, the effects of the side plates are restricted in the vicinity of the side plates and there exists almost the two-dimensional flow field in the center part of the flow. Furthermore, it is found from this figure that the fluid which is displaced by the effects of the boundary layer developed in the side plates moves to y direction along the plate rather than to the center part of the flow because of the existence of the free boundaries. For $x/b_o=4$, 8, 14 and 20, the potential core region of the jet is eaten up by the effects of diffusion of a free jet rather than that of the boundary layer formed and developed on the side plates. The saddle shaped profiles of the isotach pattern caused by the deformation of the vortex loops are observed. For $x/b_o=20$ the exess of the isotach patterns becomes calm, and it almost disappears for $x/b_o=35$.

As has been stated previously, the velocity field of the bounded jet is so complicated that none of calculations have not been done yet, so far as the author is aware. In this time, for trial, the velocity of the bounded jet in the far field region is assumed as

$$u=U_c f(\eta)g(\zeta) \tag{2}$$

using $\eta=y/b$ and $\zeta=z/b_o$. In Eq. (2), as well as a free jet flow,

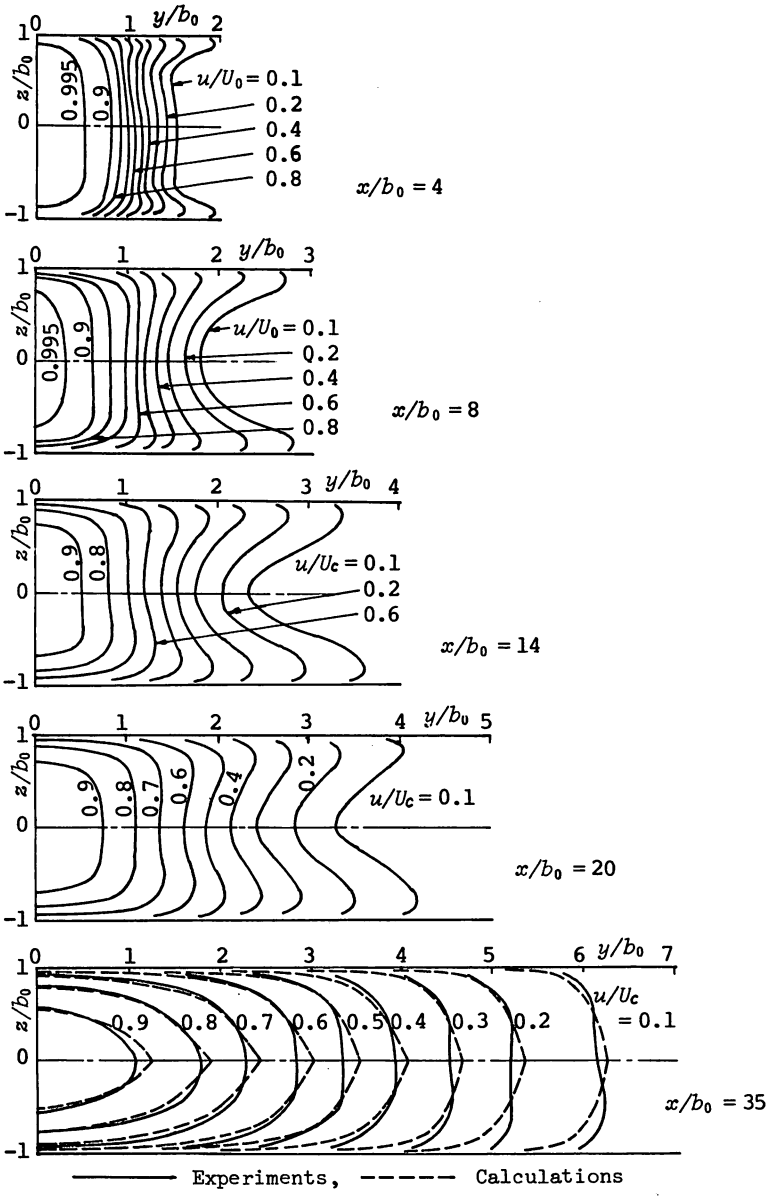

Fig. 6 Isotach patterns

$$f(\eta)=1-6\eta^2+8\eta^3-3\eta^4 \tag{3}$$

is still valid for the bounded jet and

$$g(\zeta)=(1-\zeta)^{1/7} \tag{4}$$

may be used. In the far field region, it is assumed that the width of the jet is a function of x, but not a function of z. By using the values of U_c and b shown in Figs. 4 and 5, respectively, the isotach patterns at $x/b_0=35$ are obtained and shown in Fig. 6 by

the broken lines. The isotach patterns of experiments agree well with those of calculations. Then the flow at $x/b_o=35$ is considered to be in far region where the secondary flow almost disappears.

3.4 Momentum and energy distributions

In turbulent flow, the equation of motion in the streamwise direction is expressed by

$$u\frac{\partial u}{\partial x}+v\frac{\partial u}{\partial y}+w\frac{\partial u}{\partial z}=\frac{\partial \tau_{yx}}{\partial y}+\frac{\partial \tau_{zx}}{\partial z}, \tag{5}$$

where τ_{yx} and τ_{zx} denotes the Reynolds stresses. It is difficult to estimate the distributions of these stresses, then for the momentum and energy integral equations deduced from Eq. (5), we put

$$\frac{\partial}{\partial x}\int_0^{b_0}\int_0^{b}u^2dydz=P(x) \tag{6}$$

and

$$\frac{\partial}{\partial x}\int_0^{b_0}\int_0^{b}u^3dydz=Q(x) \tag{7}$$

assuming that both $P(x)$ and $Q(x)$ be a function of x. Furthermore, putting

$$\int_0^{b_0}\int_0^{b}u^2dydz=J_x \qquad \text{and} \qquad \int_0^{b_0}\int_0^{b}u^3dydz=E_x,$$

we call J_x and E_x, the momentum and kinetic energy functions, respectively. Integrating Eqs. (6) and (7) with respect to x, we obtain

$$J_x=\int_0^{x}P(x)dx+C_1 \tag{8}$$

and

$$E_x=\int_0^{x}Q(x)dx+C_2, \tag{9}$$

where both C_1 and C_2 are the integral constants. Figure 7 shows the experimental values

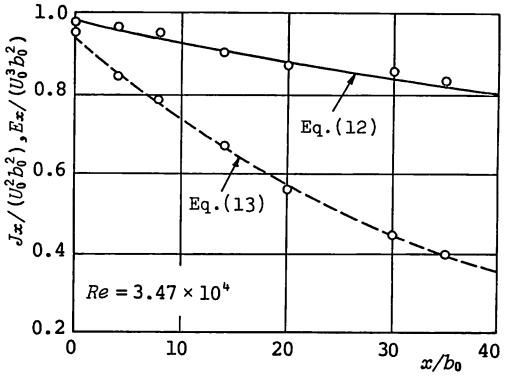

Fig. 7 Momentum and energy functions

of the momentum and kinetic energy functions normalized by those at the nozzle exit. It must be noted that the values at the nozzle exit are not equal to unity, according to the existence of the boundary layer. In this time, assuming that

$$J_x/(U_0^2 b_0^2)=\alpha_j e^{-\beta_j x/b_0} \tag{10}$$

and

$$E_x/(U_0^3 b_0^2)=\alpha_e e^{-\beta_e x/b_0} \tag{11}$$

then determining the most probable values of α_j, β_j, α_e and β_e by referring to the experimental results, we obtain

$$J_x/(U_0^2 b_0^2)=0.98e^{-0.005x/b_0} \tag{12}$$

and

$$E_x/(U_0^3 b_0^2)=0.95e^{-0.025x/b_0}. \tag{13}$$

Figure 8 and 9 represent the momentum and kinetic energy distributions per unit depth, namely,

$$J=\int_0^b u^2 dy \qquad \text{and} \qquad E=\int_0^b u^3 dy, \tag{14}$$

respectively. The calculations are also done at $x/b_0=35$ by using Eqs. (2), (3) and (4) and by using the experimental values of U_c and b shown in Figs. 4 and 5. These are shown in Figs. 8 and 9 by the solid lines. The experimental results agree well with the calculated ones. It is considered from this fact that the velocity distribution functions $f(\eta)$ and $g(\zeta)$ expressed by Eqs. (3) and (4) are valid for the flow far from the nozzle exit, so-called in the far field region.

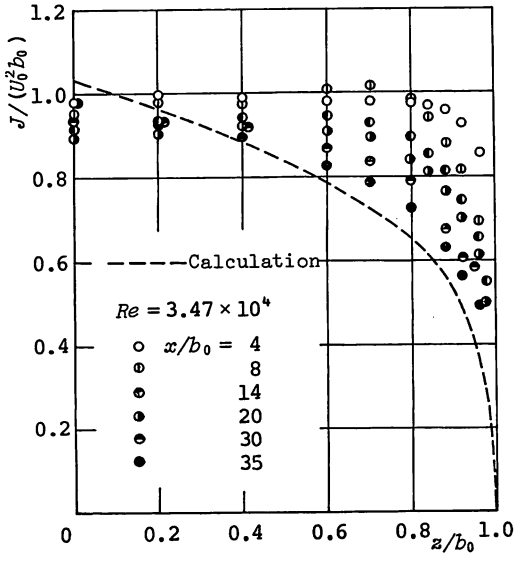

Fig. 8 Momentum distributions

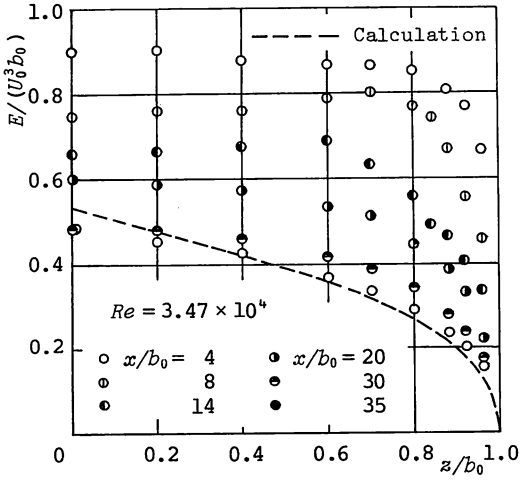

Fig. 9 Energy distributions

4. Conclusions

It was clarified from the experiments that the bounded jet flow issuing from a square nozzle is fairly influenced by the effects of the side plates for relatively small Reynolds number. The width of the jet in the mid-plane in the near field region agrees with that of a two-dimensional jet, the width of the bounded jet is smaller than that of a two-dimensional jet in the middle field region and is larger than that of a two-dimensional jet in the far field region. Three flow regions are also observed from the isotach patterns. The momentum and the kinetic energy distributions were obtained by integrating the results on the basis of the isotach patterns graphically. The results of the approximate calculations of those based on simple assumptions agree well with the experimental ones relatively far from the nozzle exit.

The author wishes to express his appreciation to Dr. Keiji Hatta (Professor, Chubu Institute of Technology), for his helpful suggestions and his interest through all phases of this research.

References

1) Hatta, K. and Nozaki, T., Bull. JSME, Vol. 18, No. 118 (1975-4), p. 349.
2) Foss, J.F. and Jones, J.B., Trans. ASME, Ser. D. Vol. 90, No. 2 (1968-6), p. 241.
3) McCabe, A., Proc. Inst. Mech. Engrs., Vol. 182, Part 3H (1967-1968), p. 342.
4) Holdeman, J.D. and Foss, J.F., Trans. ASME, Ser. I. Vol. 97, No. 3 (1975-9), p. 342.